# Chapter 5. Post-Calcined Carbon Nitride Nanosheets as an Efficient Photocatalyst for Hydrogen Production under Visible Light Irradiation

Mohammad Reza Gholipour,[a] François Béland[b] and Trong-On Do[a,*]

[a] Department of Chemical Engineering, Université Laval, Québec, G1V 0A6, Canada

[b] SiliCycle Inc., 2500, Boul. du Parc-Technologique

Québec (QC) G1P 4S6, Canada.

ACS Sustainable Chemistry & Engineering, **2017**, **5 (1)**, 213 – 220

# Résumé

La production d'hydrogène par décomposition photocatalytique de l'eau en utilisant la lumière du soleil a un énorme potentiel pour résoudre la crise mondiale de l'énergie et de l'environnement. Le défi majeur dans ce processus est de développer des photocatalyseurs efficaces qui doivent satisfaire plusieurs critères tels qu'une forte absorption du rayonnement solaire, une séparation efficace des charges et une forte stabilité photochimique. Le nitrure de carbone graphitique est l'un des meilleurs semiconducteurs pour la production de l'hydrogène en raison de la position de ses bandes de valences et de conduction ainsi que de leur gap mais aussi en raison de sa haute stabilité chimique. Cependant, il produit une petite quantité d'hydrogène sous irradiation de la lumière visible en raison de sa petite surface et de son taux de recombinaison élevés. Dans ce travail, des feuilles nanométriques de nitrure de carbone graphitique avec des lacunes en carbone ainsi que des pores ont été synthétisés par un double traitement (traitement à l'argon suivi d'une calcination à l'air). Ces feuilles de nitrure de carbone post-calcinés présentaient une activité photocatalytique beaucoup plus élevée par rapport au nitrure de carbone graphitique brut. En déposant du platine en tant que cocatalyseur via un procédé de photodéposition, ce semi-conducteur a montré une amélioration notable de son taux de production d'hydrogène, dix fois plus que le nitrure de carbone graphitique brut. Sa vitesse de production de l'hydrogène était de 5261 $\mu mol.h^{-1}.g^{-1}$ sous éclairage lumineux visible avec une efficacité quantique de 29,2% à 400 nm et 21,3% à 420 nm. Ce rendement élevé pour la production d'hydrogène pourrait être due à une plus grande surface spécifique, à une extension de l'absorption de lumière visible et à des centres de recombinaison de charge plus faibles dans tout le semi-conducteur. En outre, par étape de récurrence dans l'air, certains défauts sont introduits dans la structure des feuilles de nitrure de carbone en raison de postes vacants au carbone. Ces défauts sont considérés comme des sites photocatalytiques très actifs pour la production d'hydrogène.

# Abstract

Hydrogen production via photocatalytic water splitting using sunlight has an enormous potential to solve the worldwide energy and environmental crisis. The key challenge in this process is to develop efficient photocatalysts which must satisfy several criteria such as strong sunlight absorption, effective charge separation, and high photochemical stability. Graphitic carbon nitride is one of the best semiconductors for hydrogen evolution because of its conduction band edge, narrow band gap, and high chemical stability. However, it produces a little amount of hydrogen under visible light irradiation due to its small surface area and high recombination rates. In this work, nanosheets of graphitic carbon nitride with carbon vacancies and nanoholes were synthesized by two-step treatment process (argon treatment followed by air calcination). These post-calcined carbon nitride nanosheets exhibited much higher photocatalytic activity compared to common graphitic carbon nitride. By depositing platinum as a cocatalyst via photodeposition method, this semiconductor showed noticeable improvement in hydrogen production rate by ten times as much as graphitic carbon nitride. Its hydrogen evolution rate was 5261 μmol $h^{-1}$ $g^{-1}$ under visible light illumination with a quantum efficiency of 29.2% at 400 nm and 21.3% at 420 nm. This high amount of hydrogen production rate could be due to large specific surface area, an extension of visible light absorption tail-end and lower charge recombination centers throughout the semiconductor. In addition, by recalcination step in air, some defects are introduced into the structure of carbon nitride nanosheets owing to carbon vacancies. These defects are considered as highly active photocatalytic sites for hydrogen production.

## 5.1 Introduction

Development of technology requires a cheap and accessible source of energy. Although fossil fuels are the most well-known sources of energy for their low cost and availability, they have some important issues for human mankind such as emitting a high amount of carbon dioxide into the atmosphere which is believed to be the main reason of the greenhouse effect and climate change. Others claim that fossil fuel resources are limited and cannot be recovered once they are used. Therefore, researchers have tried to find other alternatives for fossil fuels and the best option is solar energy.

Solar energy is abundant and only a very small amount of it can provide all the energy demands of humanity around the world for one year.[16, 77] Moreover, this source of energy is renewable and sustainable, which means there is no way to over-consume it in present or future. Interestingly, sunlight energy is environmentally friendly and it doesn't produce any harmful gases as a result we won't have any climate crisis in the future.[16] However, using this source of energy is quite expensive and so it is very difficult to utilize it in large scale applications.

Hydrogen molecules can act as an energy carrier in order to store solar energy and use it later. One of the best promising ways to produce hydrogen energy is splitting water into hydrogen and oxygen with the photocatalytic process. A photocatalyst is a semiconductor that can absorb sunlight energy and generate excited electrons and holes. These charge carriers can perform redox reactions with water molecules and so generate hydrogen and oxygen.[326] One of the best photocatalysts for using solar energy is graphitic carbon nitride (g-$C_3N_4$), because of its low band gap energy that can utilize visible light to produce hydrogen from water.[312, 327]

Graphitic carbon nitride (g-$C_3N_4$) is a semiconductor consisting of tri-s-triazine units positioned in a two-dimensional graphitic-like polymer structure.[152] Due to its proper conduction band-edge position and narrow band gap, which is between 2.7-2.9 eV corresponding to wavelengths of 460-430 nm, it can generate hydrogen from water splitting under visible light irradiation.[153, 328] However, its quantum efficiency is very low mainly due to its small specific surface area and rapid charge recombination rate.[151, 329] The main synthesis method of g-$C_3N_4$ is a thermal condensation (at 500-550°C for 2-4 h) of nitrogen-rich precursors such as cyanamide, dicyandiamide, urea, and melamine.[77, 153, 330] Thermogravimetric analysis (TGA) exhibits that

g-$C_3N_4$ is stable up to 600°C even in the air, but becomes slightly unstable above this temperature, and at 700°C, it completely disappears even under an inert gas condition.[328, 331, 332]

Various methods and techniques were proposed in order to enhance the photocatalytic activity of g-$C_3N_4$ and they can be classified into four main groups as electronic structure modulation, nanostructure design, crystal structure engineering and heterostructure construction.[153, 329]Some of them such as synthesizing nanosheets of g-$C_3N_4$ can enhance hydrogen evolution significantly due to high specific surface area, enhancing charge carriers mobility and providing less charge recombination centers.[167, 169, 333, 334] In this work, a facile two-step synthesizing method for the synthesis of g-$C_3N_4$ nanosheets with some carbon vacancies and micropores is proposed that can considerably increase hydrogen production under visible light illumination. This photocatalyst showed a quantum efficiency of 29.20% at 400 nm, which is among the highest quantum efficiencies that have been reported, previously.

## 5.2 Experimental section

### 5.2.1 Sample Preparation

Bulk g-$C_3N_4$ was synthesized from dicyandiamide as reported in other literature.[156, 168, 335] Briefly, the precursors were calcined in a muffle furnace at 550°C in air for 4 h. Then, the obtained bulk g-$C_3N_4$ (GCN) was washed with distilled water several times. After this step, the photocatalyst was heated to 650°C under argon gas flow of 200 ml/min for 2h (argon treatment of g-$C_3N_4$, noted as AGCN). After this stage is completed, the obtained material was calcined again in the air, in a muffle furnace at 500°C for 2hr (recalcination of AGCN of g-$C_3N_4$ in air, noted as SGCN). Then, the material was washed several times with water to remove contaminants and dried in an oven overnight at 70°C.

### 5.2.2 Characterization

Transmission electron microscopy (TEM) images of the samples were obtained on a JOEL JEM 1230 operated at 120kV. Powder X-ray diffraction (XRD) patterns of the samples were

obtained on a Bruker SMART APEXII X-ray diffractometer equipped with a Cu Kα radiation source (λ=1.5418 Å). X-ray photoelectron spectroscopy (XPS) measurements carried out in an ion-pumped chamber (evacuated to $10^{-9}$ Torr) of a photoelectron spectrometer (Kratos Axis-Ultra) equipped with a focused X-ray source (Al Kα, hν = 1486.6 eV). The UV-vis spectra were recorded on a Cary 300 Bio UV-visible spectrophotometer. Fourier transform infrared (FTIR) absorption spectra were measured with an FTS 45 infrared spectrophotometer with the KBr pellet technique. The photoluminescence (PL) spectra were measured with the Horiba Jobin Yvon Nanolog spectrofluorimeter equipped with a 450W Xenon lamp as a source, a double monochromator for both excitation and detection, and a photomultiplier tube (PMT) detector sensitive from 250 to 850 nm. Nitrogen adsorption-desorption isotherms of the samples were measured at -196°C using Micromeretics ASAP 2010 instrument. Before the measurements, the samples were outgassed under vacuum for 6 h at 150 °C. The total pore volume ($V_{pore}$) was calculated from the amount of nitrogen adsorbed at $P/P_0 = 0.95$.

### 5.2.3 Photocatalytic test

The certain amount of photocatalysts (the optimum amount was 50 mg) was added to the 100 ml of aqueous solution of 10% triethanolamine as a sacrificial reagent. After that, the mixture was purged with nitrogen for 10 min and then under the solar simulator light, 2 wt% Pt as the co-catalyst was deposited via photodeposition technique for 2 hr. Then, the cell was purged again with nitrogen for 30 min and after the sample was ready for hydrogen production test during 3-hour cycles.

The quantum efficiency of the prepared sample was calculated according to follow equations [30, 336]:

$$\text{Quantum Efficiency (QE)} = \frac{\text{Number of reacted electrons}}{\text{Number of incident photons}} \times 100 \qquad \text{(Eq. 5.1)}$$

$$= \frac{2 \times \text{Number of evolved hydrogen molecules}}{\text{Number of incident photons}}$$

## 5.3 Result and discussions

### 5.3.1 Material characterization

Figure 5.1 demonstrates a 2D nanosheet of SGCN sample after recalcination in air in different scales. Although the nanosheet length and width are more than several hundred nanometers (Figure 5.1-A,B), AFM analysis shows that the thickness of the nanosheet hardly reaches to 10 nm (Figure 5.1-G,H).[154, 155, 337] Furthermore, as can be seen in Figure 5.1-E, there are some uniform small white dots all over the nanosheets that can be described as nanoholes and carbon vacancies generated during the second calcination step in air.[337] Due to the layered structure of graphitic carbon nitride, these vacancies were created homogeneously inside of the nanosheet planes. These vacancies with a size of less than 10 nm not only can act as active sites but also they can change the bandgap of the photocatalyst by introducing additional energy levels.[63, 178, 183] It should be noted that these in-plane nanoholes can noticeably enhance mass and charge transfer across the nanosheets of SGCN during photocatalytic process.[184, 337] Moreover, ultrathin nanosheets provide shorter pathways for photoexcited charges to migrate significantly shorter distances from the bulk material to the reaction sites located on its surfaces.[23, 27, 77] In addition, carbon vacancies can act as new active edges and cross-plane diffusion channels that can greatly speed up mass transfer and the diffusion of photogenerated charge carrier.[184, 337] Therefore, charge carriers can travel shorter distances between the inside of the nanosheets and their surfaces in order to reach the active sites and so the chance of their recombination reduced dramatically. Figure 5.1-F displays an TEM image of SGCN with photodeposited platinum nanoparticles after photocatalysis reaction. It is obvious the cocatalyst particles are uniformly deposited on the surface of nanosheets of SGCN.

Figure 5.2 displays the $N_2$ adsorption/desorption isotherms of three samples: GCN, AGCN, and SACN at 77K. All of the samples showed a type IV isotherm and their adsorption capacity enhanced significantly with increasing the relative pressure ($P/P_0$: 0.9~1), The specific surface area measured by the BET technique increased considerably and reached to 160 $m^2\ g^{-1}$ for SGCN (Table 5.1). This specific surface area is much higher than those of AGCN and GCN, which were 46 and 28 $m^2\ g^{-1}$, respectively. It should be noted that the total pore volume of SGCN (1.47 $cm^3\ g^{-1}$) is around 13 times higher than that of GCN (0.12 $cm^3\ g^{-1}$). This increase in specific surface area and

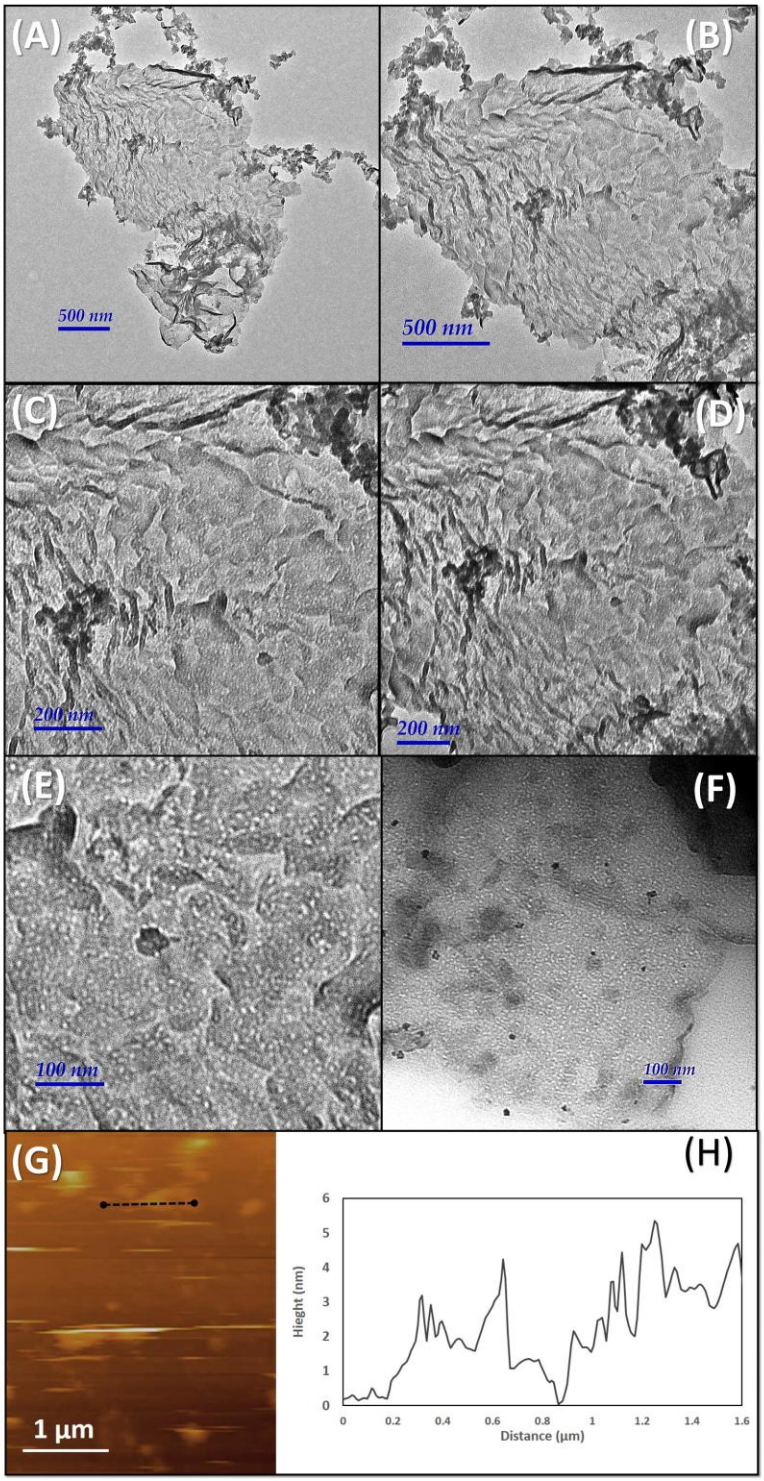


Figure 5.1. TEM images of 2-dimensional SGCN nanosheets after recalcination in air in different scales (small white dots show nanoholes inside of the nanosheet of SGCN). F) Nanosheets of SGCN with 2% Pt after photodeposition. G) Representative AFM image of SGCN and H) corresponding cross-sectional profile of typical SGCN.

total pore volume is due to a large number of in-plane holes and the crumpled structure. Furthermore, the BJH pore size distribution curves were also demonstrated in Figure 5.2-inset. Although it seems that the pore size distribution of GCN and AGCN argon-treated at 650 °C were almost similar, treatment in argon at high temperature led to having more uniform pore sizes distribution. Nevertheless, the SGCN showed a wide range of pore sizes between 1 nm and 5 nm that demonstrated the SGCN is the mixture of micropores and mesopores. These pores were mainly related to inter-particle distances and carbon vacancies throughout the SGCN nanosheets that were made during second calcination in air as described in TEM images (Figure 5.1). [158, 184, 337]

| ***Samples*** | ***Total pore volume*** ***($cm^{-3}$ $gr^{-1}$)*** | ***BET surface area*** ***($m^2$ $gr^{-1}$)*** | ***Bandgap (eV)*** | ***Hydrogen Production*** ***($\mu mol$ $h^{-1}$ $g^{-1}$)*** |
|---|---|---|---|---|
| *GCN* | 0.12 | 28.0 | 2.75 | 647.5 |
| *AGCN* | 0.52 | 45.0 | 2.56 | 771.5 |
| *SGCN* | 1.47 | 160.0 | 2.79 | 5262.0 |

Table 5.1. Total pore volume, specific surface area, band gap values, and hydrogen generation rate of GCN, AGCN and SGCN

Figure 5.3 shows the XPS spectra of the bulk sample (GCN) after different treatments; argon treatment (AGCN), followed by calcination in air (SGCN). As seen in Figure 5.3, the C 1s and N 1s XPS spectra of GCN, AGCN, and SGCN are almost similar to each other. Nonetheless, an increase in the intensities of AGCN and SGCN illustrated that C and N atoms neighboring carbon vacancies get fewer electrons than those ones on the normal sites.[337] As seen in Figure 5.3-A, the C 1s XPS spectrum of GCN can be deconvoluted into two main peaks at 285.0 and 288.1 eV, which are attributed to C−C and N−C=N, respectively.[153] Moreover, the C 1s XPS spectra of AGCN and SGCN can be resolved into two additional peaks. The peak observed at 289.6 eV can be corresponding to the $sp^2$ carbon of tri-s-triazine units attached to the NH group ($sp^2$ C−NH). The other peak at 286.5 eV is related to $sp^3$ C atoms in the structure of carbon nitride. Furthermore, the absorptions detected around 294 eV have been assigned to the charge effect of electronic delocalization associated with the presence of conjugation.[158]

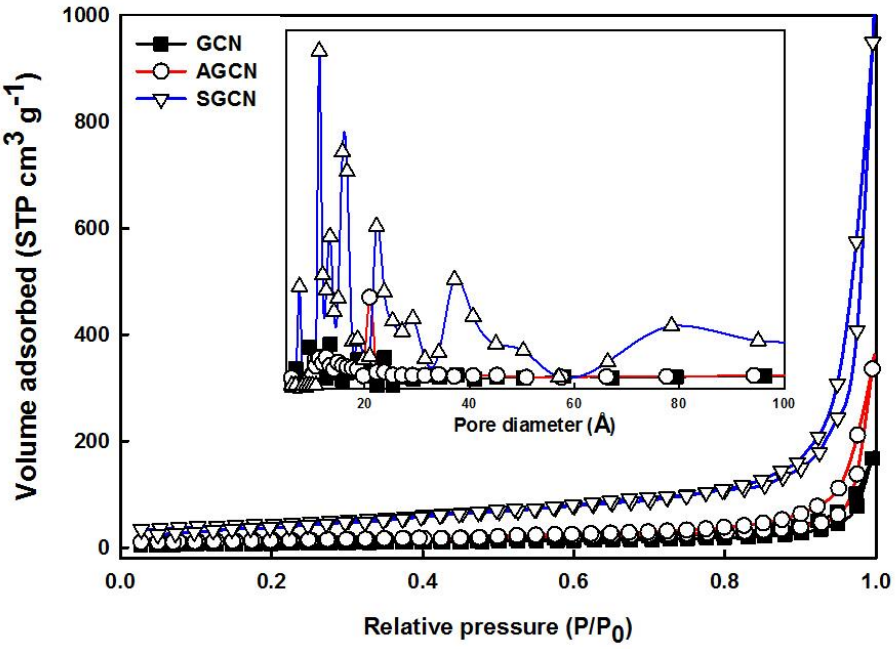


Figure 5.2. Nitrogen adsorption-desorption isotherms at 77 K and relating pore size distribution curves of GCN, AGCN, and SGCN (inset)

In the N 1s XPS spectra (Figure 5.3-B), the main curve can be divided into four peaks. The peaks located at 398.7 eV is related to the $sp^2$-bonded nitrogen in C−N=C and the peaks corresponding to the nitrogen in the tertiary group (N− $(C)_3$) are located at 400.1 eV. Moreover, the amino-functional groups with a hydrogen atom C−NH can be attributed to 401.5 eV and the absorption at 404.0 eV is due to a positive charge localization in heptazine rings.[158, 159] According to these XPS analyses, during argon treatment at high temperature some carbon atoms in the structure of GCN became loose and as a result a few of them were able to leave the bulk material and left some carbon vacancies behind in the SGCN. Following by further calcination in air, more loose carbons were able to leave carbon nitride. As a result, not only the number of carbon vacancies increased, but also some uniform nanoholes were produced.

In order to investigate the valence state of platinum as a cocatalyst, XPS analysis of Pt4f after photocatalysis reaction was conducted. The main peak of Pt 4f can be deconvoluted into two peaks at 70.4 and 73.9 eV, which are ascribed to metallic Pt 4f7/2 and Pt 4f5/2, respectively.[338-340]

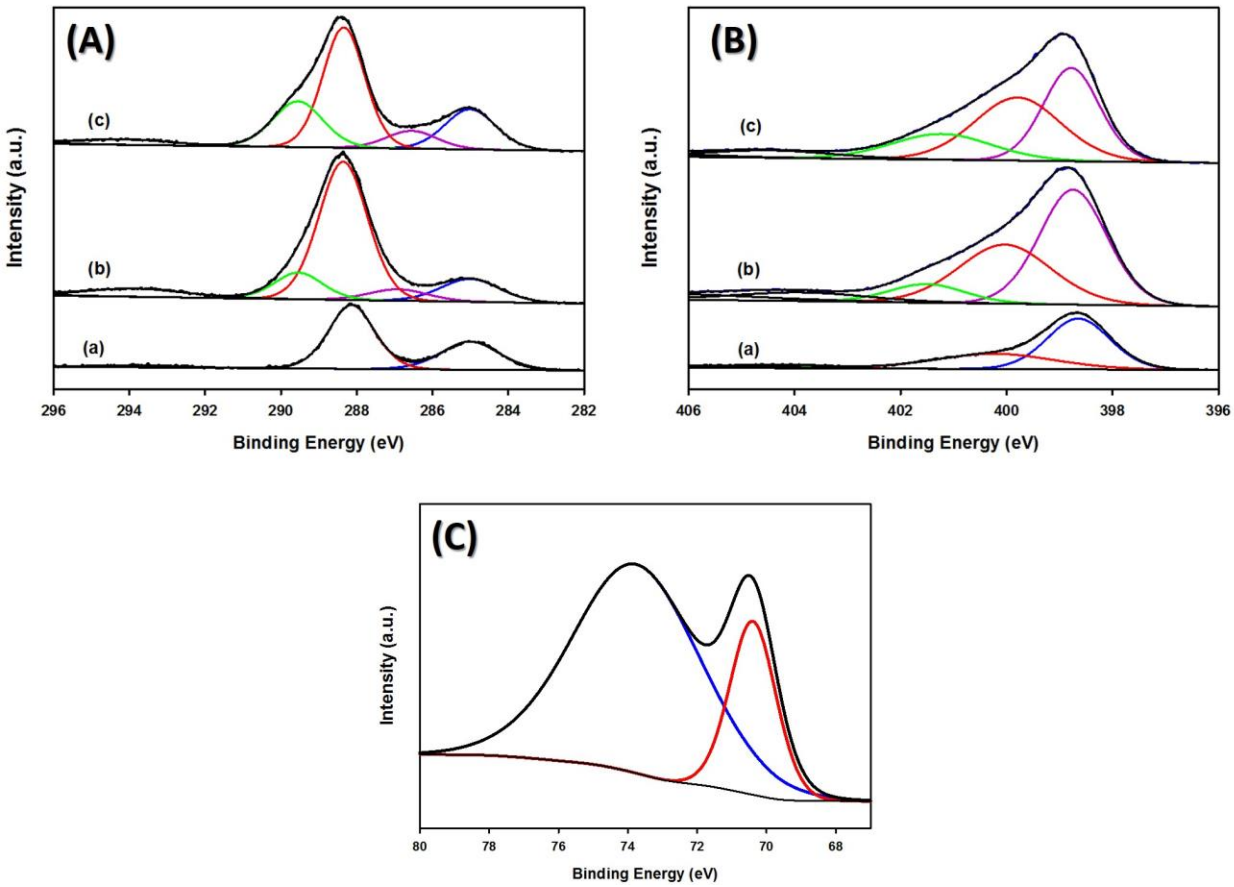


Figure 5.3. High-resolution XPS survey spectra of A) C 1s and B) N 1s for a) GCN, b) AGCN and c) SGCN. C) High-resolution XPS of the Pt4f region for Pt-SGCN photodeposited after photocatalysis

Figure 5.4 presents the X-ray diffraction (XRD) results of the synthesized bulk g-$C_3N_4$ material after different treatments. The crystal structure of bulk g-$C_3N_4$ (e.g., GCN) is shown by two main peaks of (100) and (002), which are located at 13.1° and 27.4°, respectively. The former peak ascribed to the in-plane trigonal nitrogen linkage of tri-s-triazine units and the latter one related to the periodic stacking of layers of conjugated aromatic systems. [153] The disappearance of 13.1° peak of AGCN shows that the long-range order of atomic arrangements in graphitic layers of AGCN were destroyed and as a result, AGCN can be considered as an amorphous phase of carbon nitride.[155, 158, 337, 341] In addition, the other peak with very low intensity at 27.4° indicates that we have g-$C_3N_4$ nanosheets, as displayed in TEM images. In other words, the distance between different layers of g-$C_3N_4$ increased significantly and so nanosheets of g-$C_3N_4$ were obtained.[154, 159]

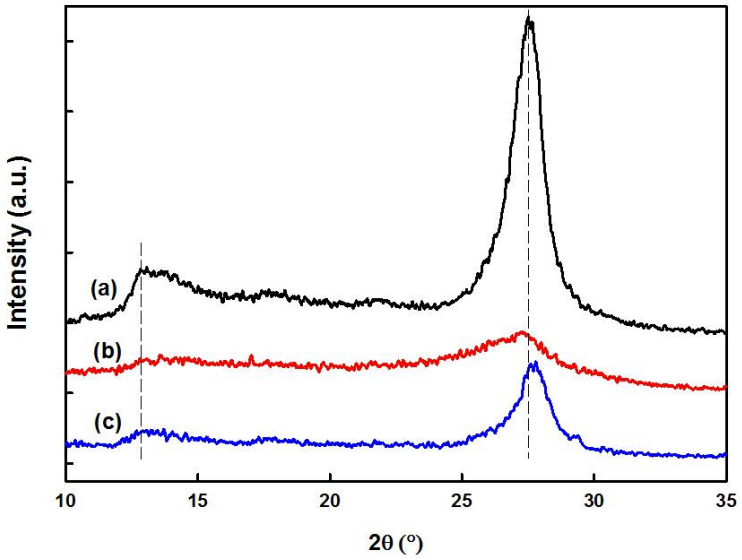


Figure 5.4. X-ray diffraction analyses of a) GCN, b) AGCN and c) SGCN

After recalcination in air (e.g., SGCN sample), the crystal structure of carbon nitride nanosheets improve moderately, and as a result, the two peaks appeared again. However, because of obtaining nanosheets and some vacancies inside of the planes of graphitic carbon nitride, the restructuring could not be completed and so the intensity of (002) peak wasn't as high as GCN. It is worth mentioning that during recalcination, most of the weak-bonded carbon and nitrogen atoms left from the bulk material in forms of various gases. These generated gases acted as a soft template in order to produce ultrathin nanosheets of graphitic carbon nitride.[167] In addition, this leaving of weak-bonded atoms generated much more vacancies and nanoholes throughout the nanosheets, which improved hydrogen generation in various ways as mentioned earlier.[156, 342]

Figure 5.5 illustrates the FTIR spectra of the GCN, AGCN, and SGCN samples to investigate their graphitic structures. The strong peak at 810 $cm^{-1}$ is attributed to the typical breathing mode of tri-s-triazine units.[145] The absorption bands between 1200 and 1700 $cm^{-1}$ region related to different stretching vibrations of heptazine-derived repeating units.[310, 343] In addition, broad peaks from 3000 to 3400 $cm^{-1}$ corresponding to N-H band, which is caused by uncondensed amino functional groups in the products.[344] There is no difference between FTIR spectra of the three materials suggesting that the nature of carbon nitride was preserved during argon treatment and recalcination in air.

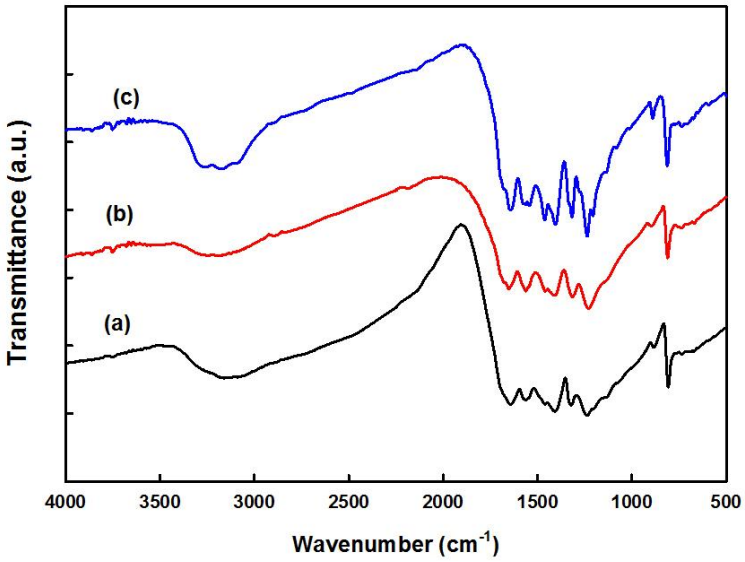


Figure 5.5. FTIR spectra of a) GCN, b) AGCN and c) SGCN

UV-visible spectroscopy is usually used in order to measure the light absorption capacity of the semiconductors and also its data can be used to calculate band structure and band gap of a photocatalyst. UV-visible spectra of GCN, AGCN and SGCN were presented in Figure 5.6. GCN can absorb visible light with a wavelength of 420 nm, because of its low band gap (2.75 eV). After argon treatment at 650°C, the UV-vis spectrum of AGCN shifted to the red region and its band gap reduced to 2.56 eV (Figure 5.6-B). Even though it could absorb visible light with a longer wavelength, it couldn't produce more hydrogen than GCN. This is due to its low crystallinity (essentially amorphous phase) and a high number of recombination centers. In addition, the band structure of AGCN seemed to not develop completely because of observing two stages in its UV-visible spectrum (the curve is different below and above 450 nm). Nonetheless, the SGCN spectrum showed that by recalcination in air, its curve shifted to blue region and so the band gap increased (to 2.79 eV). Moreover, this recalcination step helped to improve crystal structure and as a result, more charge carriers can transfer more easily across the nanosheets with limit recombination together. In addition, another absorption tail started at 430 nm to around 600 nm exhibited that the SGCN can absorb more visible light energy in comparison with GCN. It is worth mentioning that this crystallinity changes between amorphous and graphitic layer structure of nanosheets may introduce some different band energy inside the band gap structure as shown by Chen et al.[179]

These intermediate band energies can promote charge excitation as well as charge lifetime. In other words, not only charge excitation step become easier, but also photo-excited charge carriers have different stages which could help them to have less recombination process.

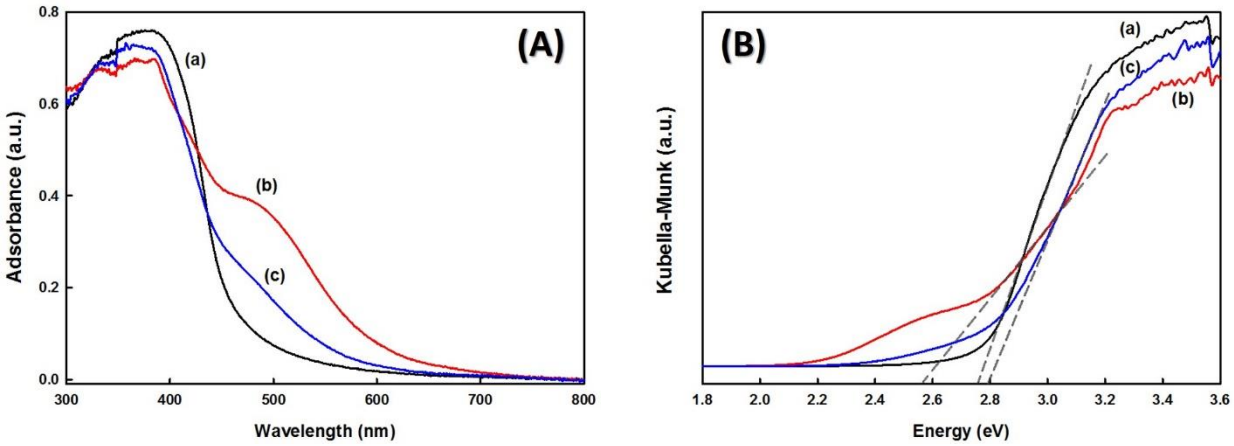


Figure 5.6. A) UV-visible absorption spectra and B) Kubelka-Munk function curves of a) GCN, b) AGCN and c) SGCN

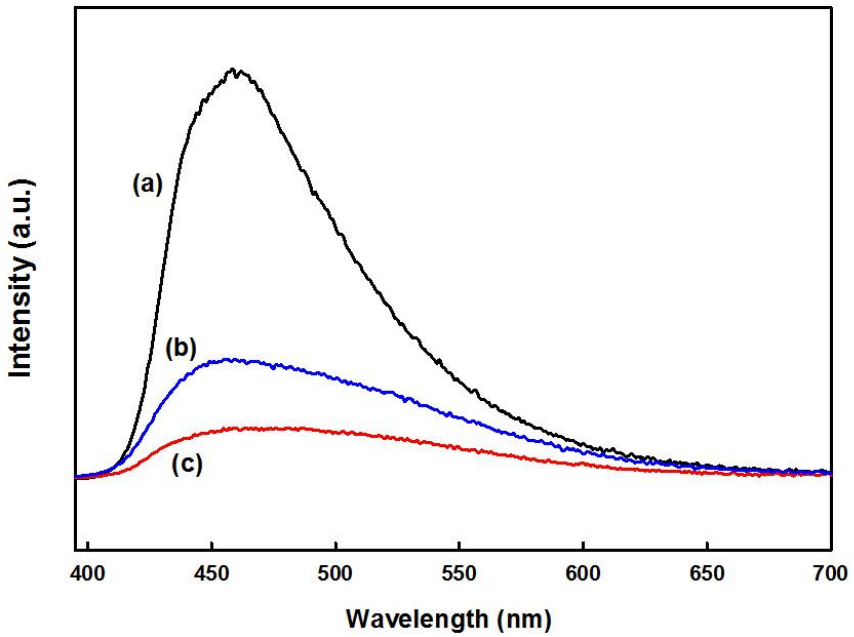


Figure 5.7. Photoluminescence spectra (390 nm excitation) of a) GCN, b) AGCN and c) SGCN (Steady state emission spectra were recorded on powdered sample under excitation wavelength of 380 nm.)

Figure 5.7 displays the steady-state photoluminescence spectra of all three samples. The prepared bulk GCN showed the highest peak intensity with respect to AGCN and SGCN relating to high radiative recombination of photoexcited electrons and holes.[155, 179, 345] In contrast, SGCN exhibited the lowest peak intensity, suggesting much lower charge recombination process during photocatalytic activity.

### 5.3.2 Photocatalytic hydrogen production

Figure 5.8-A demonstrated the hydrogen production of the three samples: GCN, AGCN and SGCN via solar simulator system with full spectrum. As seen in Figure 7-A, AGCN could only improve slightly hydrogen generation compared to that of GNC. However, SGCN could enhance hydrogen evolution more than eight times higher than GCN (5261 μmol $h^{-1}$ $g^{-1}$ for SGCN and 647 μmol $h^{-1}$ $g^{-1}$ for GCN). This considerable increase in hydrogen generation is mainly due to the presence of carbon vacancies, the high surface area and the extension tail of light absorption. The carbon vacancies not only can act like trapping spot for excited charge carriers, but also they promote mass transfer between nanosheets that help to have a higher hydrogen generation. Furthermore, these nanoholes inside of SGCN nanosheets could act as active sites for reactants. Moreover, the improvement in the structure of SGCN after the second calcination as shown in Figure 5.4, enhance the charge mobility inside of the nanosheet of graphitic carbon nitride.

For further investigation, hydrogen generation under visible light with the same system was studied with applying a light filter that surpasses wavelengths of lower than 420 nm (Figure 5.8-B). Due to a decrease in the band gap of AGCN and the fact that it can absorb more visible light, it could produce more hydrogen than GCN under visible light irradiation. The hydrogen evolution rates were 104 and 85 μmol $h^{-1}$ $g^{-1}$ for AGCN and GCN, respectively. However, SGCN showed significantly higher hydrogen production in the same conditions in comparison with the other two samples. Interestingly, it generated 387 μmol $h^{-1}$ $g^{-1}$ hydrogen, which was about 4.5 times higher than that of GCN.

Furthermore, the quantum efficiency of SGCN was also calculated with different band-pass filters (band-pass filters at 400, 420, 460, 500 and 550 nm). As it exhibited in Figure 5.8-C, the highest quantum efficiency was 29.2% which was obtained at 400 nm. This amount is among the

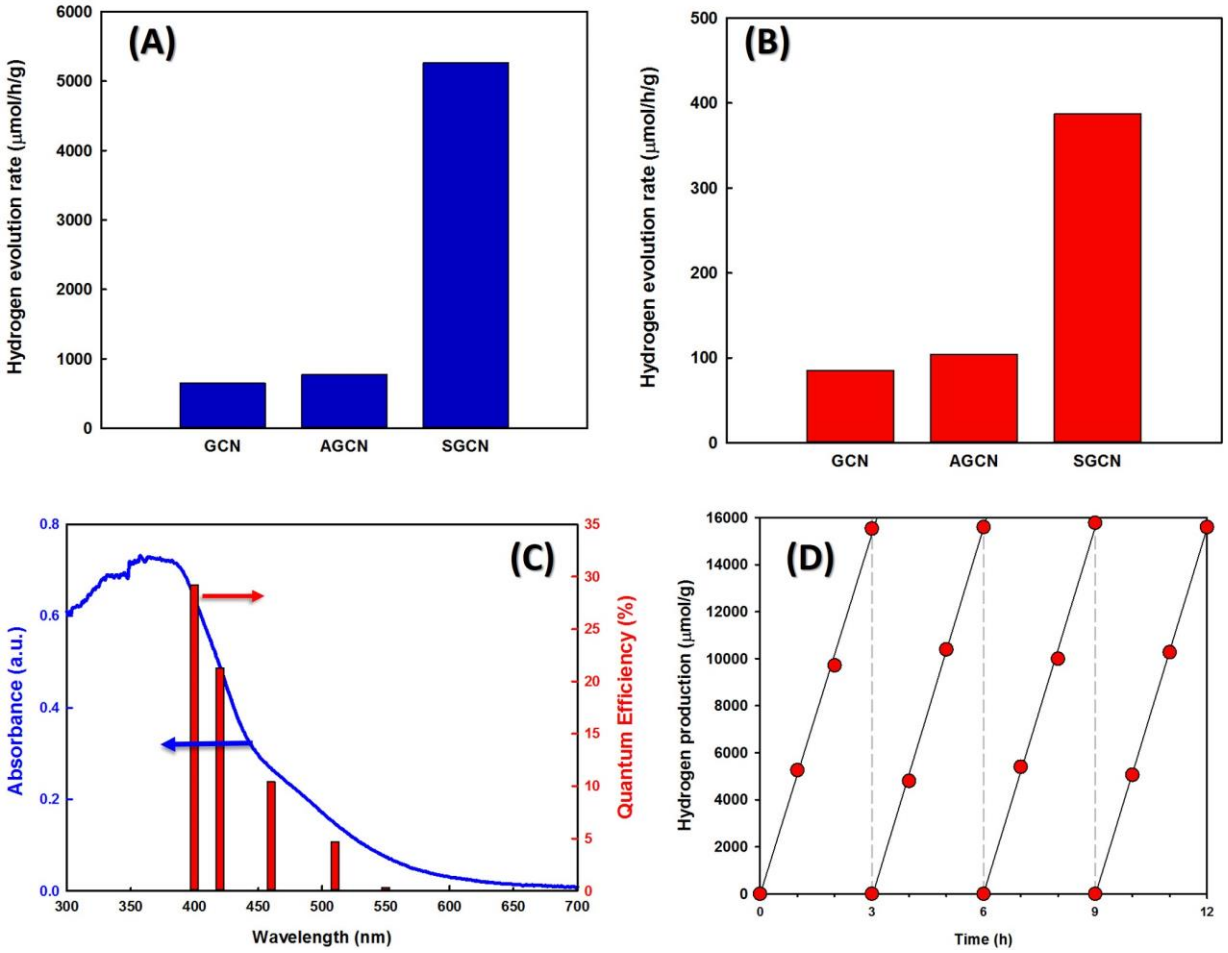


Figure 5.8. A) Hydrogen evolution rate under full spectrum via solar simulator system. B) Hydrogen generation rate under visible light irradiation with a solar simulator ($\lambda > 420$ nm).C) UV-visible spectrum and quantum efficiency of the SGCN sample. D) Hydrogen production of the SGCN for 4 cycles. Reaction conditions: 50 mg of photocatalyst loaded with 2 wt% of Pt cocatalyst; 100 ml of $H_2O$ containing 10 vol.% triethanolamine under simulator solar light 1.5 AM (ABET), equipped with 150 W Xe lamp.

highest quantum efficiency which was reported for graphitic carbon nitride under visible light illumination. In addition, the quantum efficiency calculated at 420 nm was 21.3% that shows very high hydrogen evolution in the visible light region. Because of the large band gap of SGCN nanosheets, the quantum efficiency decreased for longer light wavelengths and reached to almost 0.34% for 550 nm (Figure 5.8-C). Furthermore, the SGCN generated hydrogen over 12 h without any reduction in its activity for hydrogen production (Figure 5.8-D). It is worth mentioning that the SGCN has a great potential in order to combine with other semiconductors (nanocomposite

systems) and metals (as cocatalysts), because of its special properties such as large surface area and having enormous active sites all over the nanosheets of SGCN.

## 5.4 Conclusion

Photocatalytic hydrogen evolution from sunlight energy is one of the best options to replace with fossil fuels. Graphitic carbon nitride is one of the best photocatalysts for hydrogen production under the visible light because of its low band gap that can absorb the energy of light in a visible region. By synthesizing post-calcined nanosheets of graphitic carbon nitride with facile two-step calcination (argon treatment followed by air recalcination), ultrathin nanosheets of carbon nitride with carbon vacancies and nanoholes were obtained. This photocatalyst showed considerably high specific surface area (160 $m^2/g$) and better crystallinity compared to the amorphous phase of carbon nitride. Existing of nanoholes and carbon vacancies throughout the nanosheets caused to have more active sites for reactants as well as more charge trapping centers that can reduce charge recombination process. By applying platinum as a cocatalyst, this new photocatalyst could generate hydrogen at a rate of 5261 $\mu mol\ h^{-1}\ g^{-1}$ under sunlight irradiation. Moreover, the hydrogen evolution rate under visible light ($\lambda \geq 420$ nm) was around 387 $\mu mol\ h^{-1}\ g^{-1}$. In order to compare this novel photocatalyst with graphitic carbon nitride the quantum efficiency (Q.E.) of the band-pass filter was calculated. The Q.E. at 400 nm was 29.2% and at 420 nm was 21.3%. These values are among the highest quantum efficiencies that were reported for graphitic carbon nitride under visible light illumination.